Int. J. Electrochem. Sci., 15 **(2020)** 8761 – 8770, doi: 10.20964/2020.09.51

International Journal of
ELECTROCHEMICAL
SCIENCE
www.electrochemsci.org

Persulfate Promoted $ZnIn_2S_4$ Visible Light Photocatalytic Dye Decomposition

Deling Yuan[1], *Mengting Sun*[1], *Mengzhen Zhao*[1], *Shoufeng Tang*[1,*], *Jinbang Qi*[1], *Xiaoyu Zhang*[1], *Kai Wang*[2], *Bing Li*[3]

[1] Hebei Key Laboratory of Heavy Metal Deep-Remediation in Water and Resource Reuse, Hebei Key Laboratory of Applied Chemistry, School of Environmental and Chemical Engineering, Yanshan University, Qinhuangdao 066004, P. R. China
[2] School of Electrical Engineering, Qingdao University, Qingdao, 266000, P. R. China
[3] Department of Chemical & Materials Engineering, Faculty of Engineering, The University of Auckland, Private Bag, 92019, Auckland, New Zealand
[*]E-mail: tangshf@ysu.edu.cn

Received: 10 April 2020 / *Accepted:* 6 July 2020 / *Published:* 10 August 2020

In this work, a synergistic way for promoting the $ZnIn_2S_4$ nanoparticle photocatalysis coupled with persulfate (PS) under LED visible light was proposed. The $ZnIn_2S_4$ nanoparticle was prepared through a hydrothermal procedure and studied by diversified characterizations. When 1 mmol/L PS was added, 86% of methyl orange (MO) with the beginning amount of 15 mg/L was decolorized at the $ZnIn_2S_4$ dosage of 0.2 g/L and pH of 6 after 120 min treatment. The $ZnIn_2S_4$/PS process presented a good stability during five cyclic utilizations. Besides, the scavenger addition tests proved the sulfate radical and superoxide radical were the main species for the MO elimination. The chemical oxygen demand and total organic carbon results indicated that the synergistic system could improve the degradation and mineralization effects for the MO. In summary, the coupling $ZnIn_2S_4$/PS system presented a favorable synergistic photocatalytic performance, which not only could improve the separation of electron and hole and then activate PS, but also promote the decomposition of MO.

Keywords: $ZnIn_2S_4$; Photocatalysis; Visible light irradiation; Persulfate; dye removal

1. INTRODUCTION

Nowadays, the increase of dye wastewater lead to high human and environmental health risks because they are chemically stable, non-biodegradable, and potentially persistent in nature [1]. Many techniques are usable to reduce dyestuffs from water, such as adsorption [2], biotreatments [3], and advanced oxidation processes (AOPs) [4]. The AOPs is deemed as the efficient method because it can decompose and mineralize organic molecules completely and quickly [5]. Photocatalysis [6], Fenton [7]

and catalytic ozonation [8] have been well researched as the representative AOPs. Among them, the photocatalytic technology could utilize solar power to decompose organic matters with eco-friendly, which is proved to a prospective technique for organic wastewater treatment. Furthermore, the LED light source has become eye-catching in the photocatalysis with low-energy, feasible, and reliable properties in recent years [9].

Semiconductor material $ZnIn_2S_4$, as a ternary sulfide, has moderate band gap, favorable visible light absorption, and physicochemical durability [10], which is a benign photocatalyst for hydrogen generation and organics oxidation processes [11, 12]. However, the relatively low performances of for light absorption and charge separation efficiencies limit the application of $ZnIn_2S_4$ in photocatalysis [13].

As a newly-developing oxidizer, persulfate (PS) is widely used for organics degradation in wastewater and contaminated soil due to its strong oxidation potential (2.1 V) [14, 15]. Besides, sulfate radical ($\cdot SO_4^-$) can be generated from PS activation by UV light, heat, ultrasonication, transition metals anions, and metal oxides [16]. $\cdot SO_4^-$ has the higher oxidation capability (2.5–3.1 V) and longer life span than hydroxyl radical (·OH) [17, 18], which could decompose most of organic pollutants in water without secondary pollution. In addition, as an electron sacrificial agent, PS could promote the photo-induced charge separation in photoelectrochemical process [19].

Hence, a synergistic system introducing persulfate (PS) into a $ZnIn_2S_4$ nanoparticle photocatalytic system under LED visible light was studied to promote the removal of methyl orange (MO). A hydrothermal method was used to prepared the $ZnIn_2S_4$ photocatalyst, and its physicochemical and photoelectrochemical properties were determined through a series of characterization methods. The influencing factors on the MO decolorization, such as the PS amount, $ZnIn_2S_4$ dosage, original pH, recycle times, and scavenging additions were explored in the $ZnIn_2S_4$/PS photocatalytic process. Furthermore, the synergistic mechanism was proposed and discussed.

2. MATERIALS AND METHODS

MO, PS ($Na_2S_2O_8$), zinc sulfate ($ZnSO_4$), indium nitrate ($In(NO_3)_3$), thioacetamide (CH_3CSNH_2), tert-butyl alcohol (TBA), benzoquinone (BQ), ethanol (EtOH), disodium ethylenediamine tetraacetate (EDTA-Na_2), and p-benzoquinone (p-BQ) were of analytical grade and supplied from Sinopharm Chemical Reagent Company. All materials were used directly without being further refined. Deionized (DI) water was applied throughout the research.

The $ZnIn_2S_4$ was prepared by the hydrothermal method. The certain amounts of $In(NO_3)_3 \cdot 4H_2O$, $ZnSO_4 \cdot 7H_2O$, and thioacetamide mixed in DI water, and the mixture was transferred to a stainless-steel autoclave for heating. Then the catalyst was collected through centrifugation, washing with DI water and EtOH, and drying processes. Finally, the catalyst was uniformly grounded and stored in a desiccant drying pot.

X-ray diffraction (XRD, D-max-2500/PC), scanning electron microscopy (SEM, SUPRA55 SAPPHIRE) energy-dispersive X-ray spectroscopy (EDS), X-ray photoelectron spectroscopy (XPS, Thermo Scientific ESCA Lab 250 Xi), N_2 adsorption-desorption isotherms (ASAP2020 HD88), UV-vis diffuse reflectance spectroscopy spectrophotometer (DRS), photoluminescence (PL) spectra

fluorescence spectrophotometer, and electrochemical workstation (CHI660E) were applied to characterize the $ZnIn_2S_4$ photocatalyst.

The photocatalytic $ZnIn_2S_4$/PS was explored through the MO removal under a LED lamp (GRF30, 30 W, 400~780 nm). The calculated doses of $ZnIn_2S_4$ and PS were introduced in sequence into the prepared MO simulated wastewater (100 mL), then a 30 min dark adsorption was to achieve the reaction equilibrium before illumination. During the photocatalytic process, 1 mL solution was sampled at the certain time span from the beaker and immediately measured by the UV spectrophotometer. The MO degradation and mineralization was measured by total organic carbon (TOC, Shimadzu-VCPH) and the chemical oxygen demand (COD, DRB 200). The initial pH was regulated using 0.1 mol/L H_2SO_4 and 0.1 mol/L NaOH.

3. RESULTS AND DISCUSSION

The XRD was employed to determine the crystal texture of $ZnIn_2S_4$ nanoparticles (Fig. 1a). The diffraction peaks at 2 theta degree 21.6°, 27.7°, 32.5°, 47.2°, 52.4°, and 55.6° could be attributed the crystal phases of (006), (102), (104), (110), (116), and (022) for the $ZnIn_2S_4$ hexagon (JCPDS No. 65-2023) [20, 21]. Fig. 1b presents that the synthesized $ZnIn_2S_4$ was a uniform flower-like microspheres, which were assembled through $ZnIn_2S_4$ nanoplates, and its EDS spectrum indicated that only contained S, In, and Zn elements (Fig. 1c). Furthermore, XPS result indicated that the three of the same elements were detected in the survey spectrum (Fig. 1d). Besides, the nitrogen adsorption-desorption isotherms revealed that the isotherms for $ZnIn_2S_4$ belonged to the type IV hysteresis loop (Fig. 1e). Fig. 1f could prove that the prepared catalyst was classified as the mesopores materials, which is due to the mainly pore diameter was at 3.83 nm. In addition, the BET surface area and pore volume of $ZnIn_2S_4$ were 114.345 m^2/g and 0.245 cm^3/g, respectively.

The photo-generated carrier separation performance of $ZnIn_2S_4$ was evaluated by a series of photoelectrochemical measurements. As shown in Fig. 2a, the average photocurrent was generated and gradually stabilized when the light source was turned on, and substantially reduced to the minimum when the light source was turned off, and the average current intensity was about 0.7 μA cm^{-2}. Fig. 2b is the radius of curvature of the electrochemical impedance curve for the $ZnIn_2S_4$, which can be used to visually reveal the separation degree of photogenerated electron-holes. The PL spectra in Fig. 2c could be used to determine the photoinduced carriers trapping and separation in the catalyst.

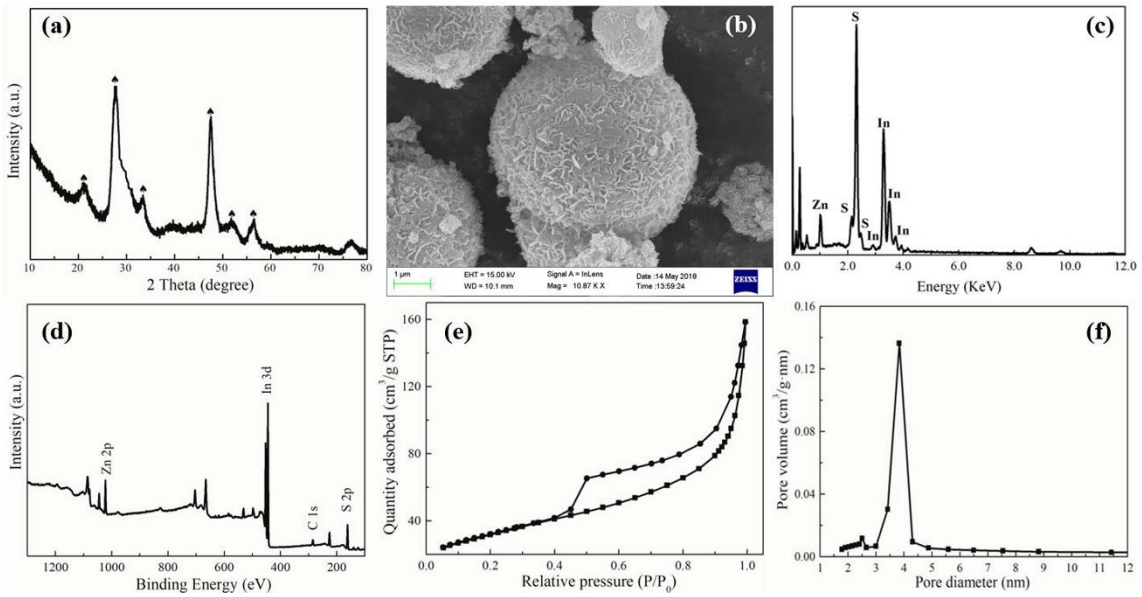

Figure 1. $ZnIn_2S_4$ characterizations: (a) XRD, (b) SEM, (c) EDX, (d) XPS, (e) N_2 adsorption-desorption isotherms, and (f) pore size distribution curve.

It can be observed that the $ZnIn_2S_4$ was excited at 550 nm, which demonstrated that it has a well visible light response. Fig. 2d illustrates the UV-vis DRS of $ZnIn_2S_4$, which showed that its maximum absorption wavelength was 580 nm.

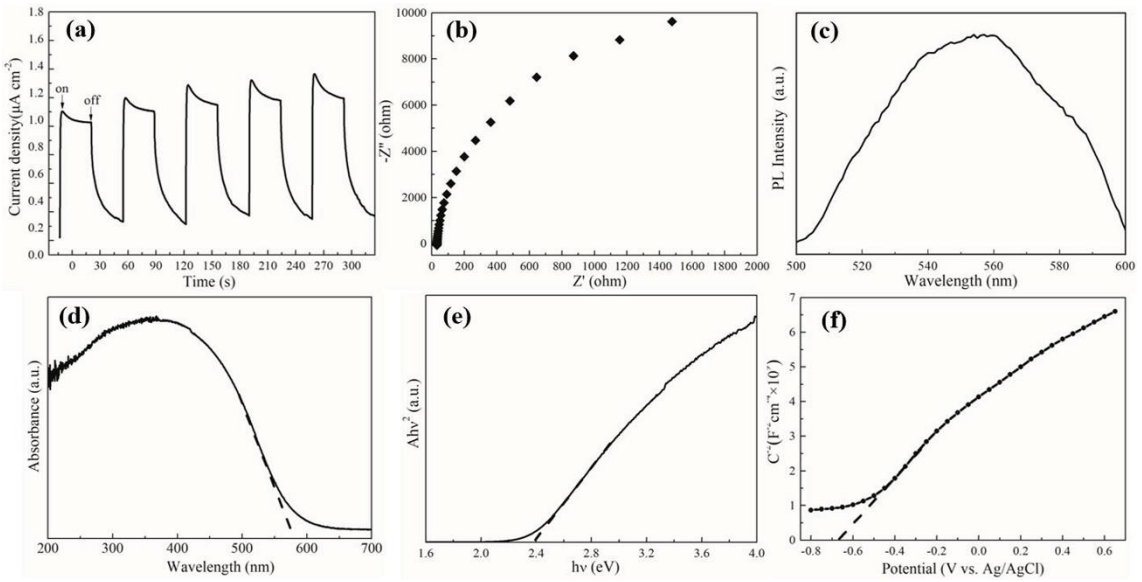

Figure 2. $ZnIn_2S_4$ measurements: (a) transient photocurrent density, (b) electrochemical impedance spectroscopy, (c) PL spectra, (d) UV-Vis diffuse reflectance spectra, (e) Tauc plot, and (f) Mott-Schottky plots.

The Tauc plot presented that the photocatalyst band distance was 2.39 eV (Fig. 2e). The Mott-Schottky measurement could be applied to analyze the band structure of $ZnIn_2S_4$ (Fig. 2f). The data plots

indicated that the catalyst belonged to n-type semiconducting material, and its flat-band potential was about -0.68 eV νs NHE. On the basis of the consequences of DRS spectrum and following eq. 1 [22], the $ZnIn_2S_4$ valence band positions was computed to be 1.71 eV. Above determination results proved that the prepared $ZnIn_2S_4$ possessed a good ability to separating photoinduced electron-holes under LED irradiation.

$$E_g = E_{VB} - E_{CB} \quad (1)$$

The comparison of the MO decolorization efficiency by different systems was displayed in Fig. 3a. The reaction was carried out at pH of 6, MO amount of 15 mg/L, PS dose of 1 mmol/L, and $ZnIn_2S_4$ addition of 0.2 g/L. The MO adsorption on the $ZnIn_2S_4$ was not significant in the dark condition during 120 min treatment. Besides, the MO decolorization ratio was only 29% by the photocatalyst under the LED visible light. The MO removal by PS alone in dark reached 37%, and only increased to 43% after irradiating by light irradiation, implying that the LED light is hard to activate PS. However, the MO decoloring efficiency achieved 86% in the $ZnIn_2S_4$/PS system after 120 min reaction. This result demonstrated that $ZnIn_2S_4$ and PS could form synergistic effect to improve the MO decolorization under LED irradiation.

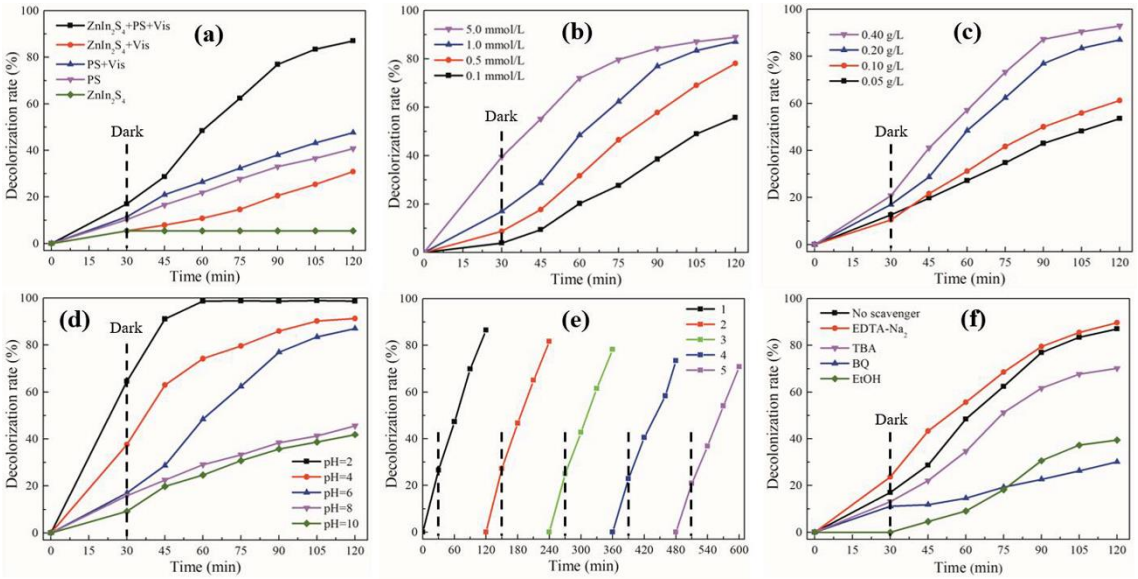

Figure 3. Decolorization effect of MO under different (a) reaction systems, (b) PS concentration, (c) catalyst dosage, (d) initial pH, (e) photocatalytic cycles, and (f) scavenger additions.

The effect of PS introduction on the MO removal in the $ZnIn_2S_4$/PS was conducted under the following experimental conditions: pH 6.4, 15 mg/L MO, and 0.2 g/L photocatalyst. Fig. 3b displays that the MO removal was enhanced with the increasing PS dose. The decolorization efficiencies were 86% and 88% when the PS dosage 1 mmol/L and 5 mmol/L after 120 min, separately. After opening the LED light, the decolorization rates were accelerated than those in the dark reaction period. More PS addition, the oxidation ability would be improved. Moreover, the added PS could be activated to generate $\cdot SO_4^-$, leading to the dye removal promotion [23, 24].

Fig. 3c presents the impact of $ZnIn_2S_4$ dose on the MO removal in the $ZnIn_2S_4$/PS, and the reaction conditions were the as follows: pH 6.4, 15 mg/ MO, and 1 mmol/L PS. The decolorization effect augmented with the increasing $ZnIn_2S_4$ dosage under the LED light. The increased photocatalyst would increase the active sites in the material, then enhance the photocatalysis in the system. But the solution system would become turbid and weaken the light absorption when the excessive catalyst was added, which would impact the photocatalytic performance.

The MO decolorization under different beginning pH (2.0 to 10.0) for the $ZnIn_2S_4$/PS was studied (Fig. 3d). The experimental conditions were as follows: 15 mg/L MO, 1 mmol/L PS, and 0.2 g/L $ZnIn_2S_4$. As shown in Fig. 3d, the MO decolorization enhanced with decreasing pH from 10 to 2. This is because the surface of $ZnIn_2S_4$ is positively charged under the acidic conditions. Hence, there would be amount of MO adsorbed on the surface of $ZnIn_2S_4$, which could promote the MO photocatalytic removal in the acidic conditions. On the other hand, $\cdot SO_4^-$ would be easily converted into ·OH at the alkaline pH [25-27], and the activity of ·OH is lower than that of $\cdot SO_4^-$, leading to the reduction of MO decolorization at pH of 8 and 10.

Fig. 3e indicates that the stability of $ZnIn_2S_4$/PS process. After five times repeated applications, the MO decolorization of $ZnIn_2S_4$/PS process was reduced, but the removal was still higher than 70%. This result proved that photocatalyst a good stability, which could ensure that PS could be constantly activated. The loss of catalysts during the recycles was the main reason for the decreasing MO elimination [28, 29].

Fig. 3f indicates that the free radical masking experiment of $ZnIn_2S_4$/PS system. In this experiment, 1 mmol/L p-BQ, 1 mmol/L EDTA-Na_2, 30 mmol/L TBA, and 30 mmol/L EtOH were used as the retardants for hole (h^+), superoxide radical ($\cdot O_2^-$), ·OH, and $\cdot SO_4^-$, respectively [30, 31]. The addition of EDTA-Na_2 had no inhibition effect on the MO removal, but also promoted the decolorization. On the one hand, EDTA-Na_2 is acidic after it dissolved in water, which could be conductive to the adsorption and degradation during the photocatalytic reactions. On the other hand, the consumption of h^+ by EDTA-Na_2 could suppress the recombination of electron (e^-) and h^+, enhancing the production of free radicals and MO elimination. In the presences of BQ and TBA, the obvious inhibitions for the MO decolorization were observed (29% and 68%), proving that both of $\cdot O_2^-$ and ·OH could be the primary substances. After EtOH was introduced in the $ZnIn_2S_4$/PS system, an obvious suppressing was discovered (40%), suggesting that the $\cdot SO_4^-$ was also a major radical. The production of these free radicals and their transformations could be inferred according to Eqs. 2-9 [32-34].

$$ZnIn_2S_4 + h\nu \rightarrow h^+ + e^- \quad (2)$$

$$e^- + O_2 \rightarrow \cdot O_2^- \quad (3)$$

$$2\cdot O_2^- + 2H^+ \rightarrow H_2O_2 + O_2 \quad (4)$$

$$H_2O_2 + e^- \rightarrow \cdot OH + OH^- \quad (5)$$

$$S_2O_8^{2-} + 2e^- \rightarrow 2\cdot SO_4^- \quad (6)$$

$$S_2O_8^{2-} + \cdot O_2^- \rightarrow \cdot SO_4^- + SO_4^{2-} + O_2 \quad (7)$$

$$S_2O_8^{2-} + OH^- \rightarrow SO_4^{2-} + \cdot OH \quad (8)$$

$$\cdot O_2^-/\cdot SO_4^-/\cdot OH/\ h^+ + MO \rightarrow \text{degraded byproducts} \quad (9)$$

In summary, the impact of the active species in the $ZnIn_2S_4$/PS system from large to small was $\cdot O_2^- \approx \cdot SO_4^- > \cdot OH > h^+$. The lower valence band for the $ZnIn_2S_4$ is benefit to produce more $\cdot O_2^-$ [35],

which was the main active specie not only degrade MO directly but also take part in the PS excitation to form $\cdot SO_4^-$. Besides, ·OH could be generated by the further process of $\cdot SO_4^-$ and $\cdot O_2^-$ [36, 37]. Therefore, $\cdot O_2^-$ and $\cdot SO_4^-$ both acted the principal roles in the collaborative process. The ·OH was of minimal importance due to it derived from other active radicals' chain reactions and was susceptible to other free radicals [38, 39]. The h^+ only was an assistant because the lower valence band of the photocatalyst makes the weak oxidation of h^+ cannot form active species but only participate the reaction directly [38, 40].

The UV/Vis absorption spectrum of $ZnIn_2S_4$/PS system was shown in Fig. 4a. The illustration indicated that the color of MO transformed from orange-yellow into colorless during 2 h treatment. The absorption peak around 465 nm represents the azo bond in the MO, which was decreased with the increasing reaction time, demonstrating that the azo bond was broken by the free radicals [41, 42]. But the absorption peak intensity around 220 nm was constantly increased, proving that there were many low molecular weight organics produced in the decolorization reaction process [43, 44].

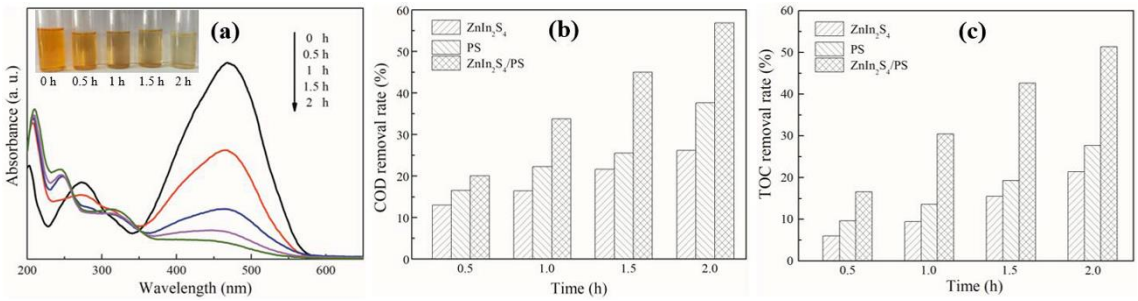

Figure 4. (a) UV/Vis absorption spectrum of MO removal in $ZnIn_2S_4$/PS. (b) COD and (c) TOC removals in $ZnIn_2S_4$, PS, and $ZnIn_2S_4$/PS.

To further clarify the MO decomposition and mineralization in the $ZnIn_2S_4$/PS system. Fig. 4b and 4c illustrates the COD and TOC removal in the $ZnIn_2S_4$, PS, and $ZnIn_2S_4$/PS systems. The COD and TOC elimination efficiencies in the solo $ZnIn_2S_4$ were 26% and 22%, respectively. While the two results were 37% and 26% by the PS alone treatment. However, the COD and TOC removals were both enhanced to 56% and 52% under the $ZnIn_2S_4$/PS process, separately. Those consequences demonstrated that synergistic effect was produced for the MO removal.

Fig. 5 displays the possible migration paths of photoexcited carriers and free radical production in the $ZnIn_2S_4$/PS system. After irradiated by LED light, e^- and h^+ would be produced by $ZnIn_2S_4$. The reductive e^- could react with O_2 absorbed on the catalyst to generate $\cdot O_2^-$. Besides, the e^- would be trapped by PS to produce $\cdot SO_4^-$ via the activation effect. In addition, $\cdot O_2^-$ also could excite PS to form $\cdot SO_4^-$, and then the formed $\cdot SO_4^-$ and $\cdot O_2^-$ could generate ·OH by the further reaction. Above evolution indicates that the coupling $ZnIn_2S_4$/PS system presented a favorable synergistic photocatalytic performance, which not only could activate PS and enhance the separation of e^- and h^+, but also promote the removal of MO.

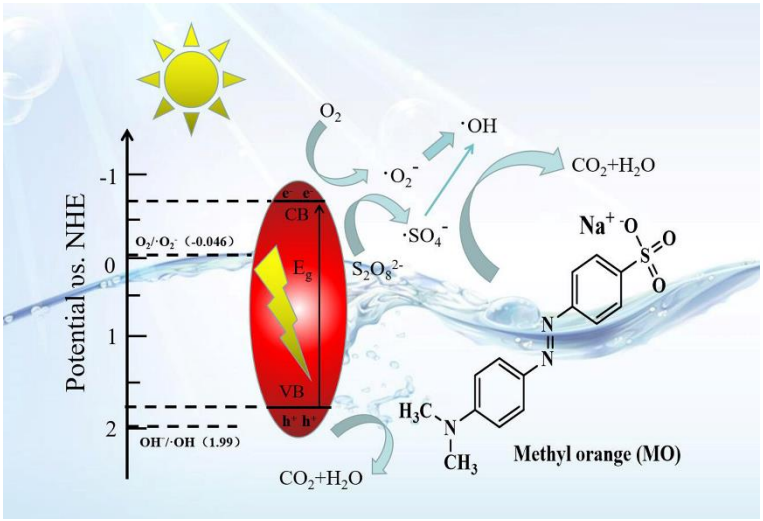

Figure 5. Possible migration paths of photogenerated carriers and active substances production in the synergistic system.

4. CONCLUSIONS

A synergy to promote the MO removal through adding the PS into $ZnIn_2S_4$ photocatalytic process under LED illumination was established. The $ZnIn_2S_4$ was successfully prepared using hydrothermal method, and its physicochemical and photoelectrochemical properties were determined through a series of characterization methods. The MO decolorization in the $ZnIn_2S_4$/PS system was raised to 86% after 120 min reaction, which was higher than those of $ZnIn_2S_4$ alone (29%) and sole PS (43%) under visible light, respectively. The effect of the active substances in the $ZnIn_2S_4$/PS process was investigated by the scavenger experiments, which verified that SO_4^- and $\cdot O_2^-$ were the primary species during the coupling process. Besides, the synergistic $ZnIn_2S_4$/PS process presented better mineralization efficiency than the other two individual systems. Lastly, the analysis of mechanism illustrated that the addition of PS could be beneficial to separate photogenerated electron-holes and improved the photocatalytic activity of $ZnIn_2S_4$ under the LED irradiation.

ACKNOWLEDGEMENTS
We are grateful to the financial supports from the National Natural Science Foundation of China (Project Nos. 51908485 and 51608468), the China Postdoctoral Science Foundation (Project No. 2019T120194), and the University Science and Technology Program Project of Hebei Provincial Department of Education (Project No. QN2020143).

References

1. D. Yuan, C. Zhang, S. Tang, X. Li, J. Tang, Y. Rao, Z. Wang, Q. Zhang, *Water Res.*, 163 (2019) 114861.

2. J. Li, B. Li, H. Huang, N. Zhao, M. Zhang, L. Cao, *Sci. Total Environ.*, 714 (2020) 136839.
3. S. Liu, S. Tsai, P. Guo, C. Lin, *Chemosphere*, 243 (2020) 125304.
4. X. Li, S. Tang, D. Yuan, J. Tang, C. Zhang, N. Li, Y. Rao, *Ecotox. Environ. Safe.*, 177 (2019) 77-85.
5. J. Li, Y. Li, Z. Xiong, G. Yao, B. Lai, *Chin. Chem. Lett.*, 30 (2019) 2139-2146.
6. S. Tang, Z. Wang, D. Yuan, Y. Zhang, J. Qi, Y. Rao, G. Lu, B. Li, K. Wang, K. Yin, *Int. J. Electrochem. Sci.*, 15 (2020) 2470-2480.
7. S. Tang, Z. Wang, D. Yuan, C. Zhang, Y. Rao, Z. Wang, K. Yin, *J. Clean. Prod.*, (2020) 122253.
8. K. El Hassani, D. Kalnina, M. Turks, B.H. Beakou, A. Anouar, *Sep. Purif. Technol.*, 210 (2019) 764-774.
9. D. Yuan, M. Sun, S. Tang, Y. Zhang, Z. Wang, J. Qi, Y. Rao, Q. Zhang, *Chin. Chem. Lett.*, 31 (2020) 547-550.
10. S. Wan, M. Ou, Q. Zhong, S. Zhang, F. Song, *Chem. Eng. J.*, 325 (2017) 690-699.
11. Y. Chen, R. Huang, D. Chen, Y. Wang, W. Liu, X. Li, Z. Li, *ACS Appl. Mater. Inter.*, 4 (2012) 2273-2279.
12. Q. Gao, Y. Han, P. Liang, J. Meng, *Phys. Chem. Chem. Phys.*, 22 (2020) 6291-6299.
13. J. Ke, M. Adnan Younis, Y. Kong, H. Zhou, J. Liu, L. Lei, Y. Hou, *Nano-Micro Lett.*, 10 (2018) 69.
14. D. Yuan, C. Zhang, S. Tang, M. Sun, Y. Zhang, Y. Rao, Z. Wang, J. Ke, *Sci. Total Environ.*, 727 (2020) 138773.
15. B. Shen, C. Dong, J. Ji, M. Xing, J. Zhang, *Chin. Chem. Lett.*, 30 (2019) 2205-2210.
16. S. Tang, J. Tang, D. Yuan, Z. Wang, Y. Zhang, Y. Rao, *RSC Adv.*, 10 (2020) 17627-17634.
17. N. Li, S. Tang, Y. Rao, J. Qi, Q. Zhang, D. Yuan, *Electrochim. Acta*, 298 (2019) 59-69.
18. H. Zhang, Q. Ji, L. Lai, G. Yao, B. Lai, *Chin. Chem. Lett.*, 30 (2019) 1129-1132.
19. N. Li, S. Tang, Y. Rao, J. Qi, P. Wang, Y. Jiang, H. Huang, J. Gu, D. Yuan, *Electrochim. Acta*, 270 (2018) 330-338.
20. Z. Guan, Z. Xu, Q. Li, P. Wang, G. Li, J. Yang, *Appl. Catal. B.,* 227 (2018) 512-518.
21. J. Wu, K. Yin, M. Li, Z. Wu, S. Xiao, H. Wang, J.A. Duan, J. He, *Nanoscale*, 12 (2020) 4077-4084.
22. C. Duan, Y. Yu, J. Xiao, X. Zhang, L. Li, P. Yang, J. Wu, H. Xi, *Sci. China Mater.*, 63 (2020) 667-685.
23. C. Bu, F. Li, K. Yin, J. Pang, L. Wang, K. Wang, *ACS Appl. Electron. Mater.*, 2 (2020) 863-878.
24. C. Wang, Q. Yang, Z. Li, K.A. Lin, S. Tong, *Sep. Purif. Technol.*, 213 (2019) 447-455.
25. R. Guo, Q. Meng, H. Zhang, X. Zhang, B. Li, X. Cheng, Q. Cheng, *Chem. Eng. J.*, 355 (2019) 952-962.
26. K. Wang, L. Li, T. Zhang, Z. Liu, *Energy*, 70 (2014) 612-617.
27. H. Zhang, Q. Ji, L. Lai, G. Yao, B. Lai, *Chin. Chem. Lett.*, 30 (2019) 1129-1132.
28. Y. Dong, L. Bian, P. Wang, *Chem. Eng. J.*, 358 (2019) 1489-1498.
29. Y. Zhou, Y. Wang, K. Wang, L. Kang, F. Peng, L. Wang, J. Pang, *Appl. Energ.*, 260 (2020) 114169.
30. Z. Dong, Q. Zhang, B. Chen, J. Hong, *Chem. Eng. J.*, 357 (2019) 337-347.
31. K. Wang, W. Li, W. Xue, S. Zhou, Y. Lan, H. Zhang, Z. Sui, *Int. J. Electrochem. Sci.*, 12 (2017) 8306-8314.
32. F. Rehman, M. Sayed, J.A. Khan, N.S. Shah, H.M. Khan, D.D. Dionysiou, *J. Hazard. Mater.*, 357 (2018) 506-514.
33. M. Gu, Q. Sui, U. Farooq, X. Zhang, Z. Qiu, S. Lyu, *J. Hazard. Mater.*, 359 (2018) 157-165.
34. T. Zhang, Y. Liu, Y. Rao, X. Li, D. Yuan, S. Tang, Q. Zhao, *Chem. Eng. J.*, 384 (2020) 123350.
35. B. Gao, L. Liu, J. Liu, F. Yang, *Appl. Catal. B.*, 129 (2013) 89-97.
36. S. Tang, D. Yuan, Y. Rao, N. Li, J. Qi, T. Cheng, Z. Sun, J. Gu, H. Huang, *Chem. Eng. J.*, 337 (2018) 446-454.
37. J. Liu, J. Zhang, D. Wang, D. Li, J. Ke, S. Wang, S. Liu, H. Xiao, R. Wang, *ACS Sustain. Chem. Eng.*, 7 (2019) 12428-12438.
38. J. Liu, J. Ke, Y. Li, B. Liu, L. Wang, H. Xiao, S. Wang, *Appl. Catal. B.*, 236 (2018) 396-403.
39. H. Xie, J. Zhang, D. Wang, J. Liu, L. Wang, H. Xiao, *Appl. Surf. Sci.*, (2019) 144456.

40. Y. Han, Q. Zhang, L. Wu, *Desalination*, 477 (2020) 114270.
41. W. Szeto, J. Li, H. Huang, D.Y.C. Leung, *Chem. Eng. Sci.*, 177 (2018) 380-390.
42. Q. Chen, L. Chen, J. Qi, Y. Tong, Y. Lv, C. Xu, J. Ni, W. Liu, *Chin. Chem. Lett.*, 30 (2019) 1214-1218.
43. P. Li, Z. Liu, X. Wang, Y. Guo, L. Wang, *Chemosphere*, 180 (2017) 100-107.
44. J. Chen, J. Zhan, Y. Zhang, Y. Tang, *Chin. Chem. Lett.*, 30 (2019) 735-738.